Alpha-synuclein fibril-based mouse model of REM sleep behavior disorder as a prodrome of Parkinson's disease

Han Soo Yoo

The Graduate School
Yonsei University
Department of Medicine

Alpha-synuclein fibril-based mouse model of REM sleep behavior disorder as a prodrome of Parkinson's disease

A Dissertation Submitted
to the Department of Medicine
and the Graduate School of Yonsei University
in partial fulfillment of the
requirements for the degree of
Doctor of Philosophy in Medical Science

Han Soo Yoo

December 2024

This certifies that the Dissertation of Han Soo Yoo is approved.

Thesis Supervisor	Phil Hyu Lee
Thesis Committee Member	Young H. Sohn
Thesis Committee Member	Chul Hyoung Lyoo
Thesis Committee Member	Sang Myun Park
Thesis Committee Member	Seung-Jae Lee

The Graduate School
Yonsei University
December 2024

ACKNOWLEDGEMENTS

I would like to express my deep appreciation to my director, Professor Phil Hyu Lee, for his help to accomplish this work in detail. Without his advice, this dissertation would not have been possible. I also appreciate Professor Young H. Sohn, Chul Hyoung Lyoo, Sang Myun Park, and Seung-Jae Lee for their concerns and complements in this research. Furthermore, I express my gratitude to all co-workers and collaborators involved in the experiment. Mostly, I would like to thank my loving family for taking care of everything and giving emotional support.

TABLE OF CONTENTS

LIST OF FIGURES

LIST OF TABLES

ABSTRACT

Alpha-synuclein fibril-based mouse model of REM sleep behavior disorder as a prodrome of Parkinson's disease

Background & Objective: REM sleep behavior disorder (RBD) is widely established as a highly predictive symptom of future alpha-synucleinopathy. The sublaterodorsal tegmental nucleus (SLD) plays a critical role in maintaining muscle atonia during REM sleep. Although the underlying mechanisms of RBD remain unknown, it is thought that RBD is cause by α-synuclein(αSyn)-mediated degeneration of the SLD neurons. Therefore, the development of a robust animal model that incorporates synucleinopathy and recapitulates RBD would offer a unique opportunity to study a prodromal phase of synucleinopathy. We investigated whether in wild-type mice, inoculation of αSyn preformed fibrils (PFFs) into the SLD would lead to either RBD or subsequent parkinsonism-like phenotype.

Methods: Human autopsy samples were used to examine the pathological burden in the SLD according to the presence of RBD in patients with Lewy body disease. Adeno-associated virus (AAV) was used to drive the overexpression of αSyn in SLD neurons to establish the causal relationship of αSyn pathology in the SLD followed by the development of RBD. Then, we stereotaxically injected wild-type mouse αSyn PFFs into the SLD in B6C3F1/J mice. At predetermined time points, mice then underwent histopathological, electrophysiological, and behavioral analyses. Co-labeling using antibodies to phosphorylated αSyn (p-αSyn) and common neurotransmitter markers was used to reveal neurons susceptible to αSyn pathology in the SLD. Neuronal and glial markers were also used to investigate the degeneration and reactive gliosis in the SLD.

Results: Immunohistochemical staining for p-αSyn revealed numerous αSyn aggregates in the SLD of PD patients with comorbid RBD, whereas aggregates were sparse or absent in the PD patients

without RBD and healthy controls. AAV-driven overexpression of αSyn in SLD neurons induced RBD-like behaviors in mice. αSyn PFF inoculation into the mouse SLD seeded endogenous αSyn pathology and initiated propagative αSyn pathology in the brain from the injection site rostrally to the cerebral cortex and caudally to the spinal cord. αSyn pathology was first found in the substantia nigra pars compacta at 6-months post-injection (mpi). Pathologic aggregates were initially found in cholinergic neurons and over time also in surrounding oligodendrocytes in the SLD. Seeded αSyn pathology in the SLD was associated with RBD-like behavior in mice from 3 mpi and also displayed cortical slowing and perturbed sleep-wake architecture from 6 mpi. Propagative αSyn pathology precipitated gait deficits at 12 mpi, especially in male mice.

Conclusion: We demonstrated that the SLD can serve as a portal for the early spread of synucleinopathy and that induction of αSyn pathology in this manner results in an RBD-like phenotype in mice. We anticipate this mouse model will be a useful tool for understanding prodromal disease mechanisms and studying disease-modifying treatment in synucleinopathy including Parkinson's disease.

Key words : REM sleep behavior disorder; Parkinson's disease; sublaterodorsal tegmental nucleus; alpha-synuclein; mouse model.

I. INTRODUCTION

Alpha-synucleinopathies including Parkinson's disease (PD) are neurodegenerative disorders differing in their clinical presentation but are unified by the deposition of α-synuclein (αSyn) aggregates in the brain.[1),2)] Pathogenic αSyn species are the main component of the hallmark inclusions that define PD,[3)] and genetic variants in the αSyn gene cause genetic forms of the disease,[4)] underscoring the relevance of αSyn in PD pathogenesis. PD is typified by its cardinal motor symptoms, which are thought to arise from αSyn aggregation in association with dopaminergic neuronal loss in the substantia nigra pars compacta.[1),5)] In this sense, recognizing the mechanistic interplay between αSyn pathology and functional neural circuits has proven crucial in enriching our understanding of neurodegenerative mechanisms, an assertion that is justified by the success of dopamine replacement therapy in treating Parkinsonian motor symptoms. However, it is apparent that synucleinopathic processes extend far beyond the nigrostriatal circuit. Indeed, αSyn aggregates are found in diverse cell types, across the central nervous system[6)] and periphery.[7)] This widespread pathological distribution reflects clinically various extranigral symptoms that together constitute the multisystem disorder that is now recognized as PD.[8)] Despite the evident role of αSyn in the pathogenesis of PD motor symptoms, an integrated etiology of its varied presentations remains elusive.

Converging lines of evidence indicate that αSyn pathology can propagate between cells in a prion-like manner, consistent with the progressive nature of PD. For instance, embryonic cell grafts in PD patients develop αSyn inclusions years after grafting, indicative of host-graft pathological spread.[9)] Furthermore, post-mortem examination of PD patients reveals that αSyn pathology follows a stereotypic, caudo-rostral progression throughout the brain with advancing disease. From this, a topographical sequence of pathology can be inferred that corresponds with the clinical progression of PD, allowing for the staging of its disease course.[6)] Notably, early involvement in the sublaterodorsal tegmental nucleus (SLD) is linked with rapid eye movement (REM) sleep behavior disorder (RBD),[10),11)] a prodrome of PD marked by the dissociation of REM sleep with its accompanying muscle paralysis.[12)] Clinical and experimental evidence give credence to this notion: post-mortem and imaging studies reveal αSyn aggregates and neuronal loss in the

SLD of RBD patients,[13),14),15),16),17)] while restricted lesions of the SLD in animals and humans result in REM sleep motor hyperactivity, the defining symptom of RBD. These observations highlight the SLD as the physiological substrate for REM sleep muscle paralysis, implicating these same cells in RBD pathophysiology.[18)] Abundant evidence supports the notion that the transcellular propagation of αSyn shapes the trajectory of PD from prodromal to clinically manifest stages of disease.

Our understanding of synucleinopathies is limited by the lack of animal models that concomitantly recapitulate pathological and behavioral features characteristic of human PD. Although the administration of neurotoxins in rodents induces dopamine neuronal loss and motor impairment,[19),20)] such models lack clinical relevance because the observed effects do not reflect underlying αSyn pathology. Conversely, current transgenic and viral-mediated models of PD successfully induce Lewy-like histopathology,[21),22)] but both rely on ectopic overexpression which distorts the distribution of αSyn aggregates in the brain, thus not lending themselves to the study of propagative αSyn pathology as observed in human PD. On the basis of the prion-like nature of αSyn pathology, recent investigations have used recombinant preformed fibrils (PFF) of αSyn to seed the conversion of endogenous αSyn into its aggregated from in vitro and in vivo. Following a single intrastriatal PFF inoculation in mice, αSyn aggregates and dopamine cell loss were observed in the substantia nigra pars compacta and were accompanied by Parkinsonian motor deficits.[23)] Furthermore, several recent studies have modeled aspects of prodromal PD by initiating caudal-rostral pathological spread at early foci of PD pathology.[24),25)] However, the specific cellular substrates implicated in RBD have yet to be fully resolved.

Given the established role of SLD neurons in regulating motor activity during REM sleep, we hypothesized that early αSyn pathology in the SLD results in RBD, which progresses into a waking Parkinsonian phenotype as pathology propagates to the substantia nigra pars compacta and the rest of the brain. Utilizing a viral vector-mediated approach, we first induced localized αSyn pathology in SLD neurons to validate their causal role in RBD symptomatology. To examine if pathological spread beyond the SLD contributes to further symptomatic progression of PD, we stereotaxically injected αSyn PFFs into the SLD of wild-type mice. Here, we demonstrated in mice that: (i) the induction of αSyn pathology in SLD neurons was sufficient to trigger RBD-like

behaviors; (ii) seeded αSyn pathology in the SLD morphologically resembled neuropathological features of human PD; (iii) its subsequent spread led to the emergence of Parkinsonian motor deficits in mice; and (iv) these animals also developed extensive sleep-wake disturbances resembling those observed in advanced PD. Therefore, our study uncovers mechanistic insights into RBD pathogenesis and highlights key pathogenic events crucial in the early progression of PD.

II. METHODS

2.1. Post-mortem human autopsy samples

Demographic and neuropathological data were ascertained from the Integrated Neurodegenerative Disease Database (INDD) in the Center for Neurodegenerative Disease Research (CNDR) at the University of Pennsylvania. First, we enrolled 20 cases who (1) were clinical diagnosed as Parkinson's disease or Parkinson's disease with dementia, (2) were neuropathological diagnosed as Lewy body disease, and (3) had the information on RBD. The presence of RBD was determined if the patient had an RBD screening questionnaire score of 7 or higher,[26] was confirmed by video-polysomnography, or reported dream enactment behavior by the patient of the patient's bed partner. After excluding cases who had a borderline RBD screening questionnaire score (4 to 6) or had a poor quality of autopsy sample, we finally enrolled 10 LBD cases and grouped 6 cases as the RBD positive (PD-RBD) group and 4 cases as the RBD negative (PD+RBD) groups. We also enrolled 4 control cases whose primary neuropathological diagnosis was either unremarkable or primary age-related tauopathy. Paraffinized post-mortem brain samples were available for all cases. Detailed demographic information on these patients was described in Table 1. The use of post-mortem tissue was approved by the Institutional Review Boards of the University of Pennsylvania. Patients or their next of kin provided written informed consent for autopsy and the use of tissue samples.

Table 1. Demographic characteristics of post-mortem human autopsy samples

	Healthy controls	PD patients without RBD	PD patients with RBD	p-value
Number	4	4	6	
Age at death, yr	74.1 ± 7.5	81.8 ± 9.7	73.1 ± 5.9	0.220
Sex, male, n (%)	3 (75.0)	2 (50.0)	5 (83.3)	0.511
Post-mortem interval, month	19.0 ± 13.5	12.8 ± 8.6	22.7 ± 18.3	0.603
Brain weight, g	1292.5 ± 318.5	1210.0 ± 89.1	1381.8 ± 61.8	0.354

The values are expressed as mean ± standard deviation or number (percentage). P-values are results of the independent *t* test for continuous variable and the Fisher's exact test for categorical variable.

2.2. Animals and ethics statement

All experimental protocols were jointly approved by Institutional Animal Care and Use Committees. Male and female wild-type mice of C57BL/6 or B6C3F1/J genetic background were used for AAV-αSyn and PFF injections. To account for confounding effects of age or biological sex, experiments were performed on young adult mice of both sexes (age: 10 ± 4 weeks; mass: 23 ± 3g depending on sex). Food and drinking water were provided ad libitum, and mice were maintained on a 12:12 light-dark cycle (lights on 07:00-19:00).

2.3. AAV and PFF injection materials

An AAV2 serotype was used to overexpress wild-type human αSyn under the chicken beta-actin promoter (AAV-αSyn; construct: AAV2-CBA-αSyn) in all SLD neurons. For control experiments, mice were injected with viruses encoding for an inert green fluorescent protein, in place of αSyn (AAV-GFP). AAV-αSyn was acquired from the Michael J. Fox Foundation.

Wild-type recombinant αSyn protein was produced, purified, and assembled into fibrils as described previously.[23] Briefly, full-length wild-type mouse αSyn constructs were expressed in E. coli BL21 (DE3) RIL cells (Agilent Technologies #230245) and proteins were purified following lysis using size exclusion and anion exchange chromatography. Then, αSyn protein (monomer) was concentrated to 5mg/mL and kept frozen until use. To synthesize recombinant αSyn PFFs in vitro, αSyn monomer was agitated in a thermomixer (Eppendorf) at 1000 rpm at 37 Cº for 7 days. Successful fibril formation was validated through electron microscopy, sedimentation assay, and Thioflavin S staining as described previously.[27] Prior to stereotaxic injection, PFFs were briefly sonicated for 10 cycles (30 sec ON, 30 sec OFF, high intensity) in a bath sonicator (Diagenode Bioruptor Plus or Qsonica Q125 with cup horn attachment) to ensure fibrils were of appropriate size to elicit a pathogenic response in vivo.

2.4. Stereotaxic inoculation of mouse brains

Intracerebral injections of AAVs or PFFs into the murine SLD were performed as previously described.[28] Adult mice of 3-4 months of age were anesthetized then secured into a stereotaxic frame (David Kopf Instruments, USA), before a craniotomy was performed to expose a 1mm

opening in the skull above the SLD. AAV infusions were performed to a total volume of 400nL (200nL per hemisphere) bilaterally at 50nL/min into the SLD (stereotaxic coordinates: AP = -5.20mm, ML = ± 0.9mm, DV = -4.25mm from bregma), using a digital microinjection syringe pump (Harvard apparatus). PFF injections were performed to a total volume of 500nL unilaterally at a rate of 100nL/min into the right SLD, using a 10-μL syringe (Hamilton, gauge size 33, bevel 45°). Mice were administered postoperative analgesic and recovered for at least 14 days after the surgery.

2.5. EEG and EMG electrode implantation

For the evaluation of sleep-wake behaviors, mice were instrumented with electroencephalographic (EEG) and electromyographic (EMG) electrodes, which respectively allow for cortical and muscle activity measurements.[28),29)] Electrodes were fashioned with stainless-steel wire, soldered onto a microstrip conductor, and assembled into a headplug. Depending on the experiment, mice were instrumented at 2 weeks post-AAV injection or 10 weeks post-PFF injection, to allow for recording of sleep-wake behaviors at predetermined timepoints. During EEG/EMG instrumentation, animals were prepared as described above and elsewhere, then transferred onto a stereotaxic apparatus under anesthesia. Four craniotomies were performed to allow for attachment of EEG electrodes onto the skull with stainless-steel miniature screws (J.I. Morris), and the headplug was then secured using dental cement (C&B Metabond and 3M Ketac Cem). EMG electrodes were sutured into the neck and right masseter muscles. Mice were administered postoperative analgesic and recovered for a minimum of 14 days before behavioral experiments.

2.6. Sleep-wake recordings

Experiments involved recording EEG, EMG, and video data to monitor sleep-wake behavior and allow for the identification of potential RBD-like behaviors in mice. Following recovery from EEG/EMG implantation surgeries, mice were transferred to sound-attenuated recording enclosures and their implants were connected with a lightweight cable to a Physiodata Amplifier system (Grass 15LT, Astro Med.) for data acquisition. Electrophysiological signals were amplified by 500-1000x, digitized at 1000Hz (Spike2 Software, 1401 interface, Cambridge Electronic Design Ltd.)

and band-pass filtered (EEG, 0.1-1000Hz; EMG, 30-3000 Hz). Prior to data analysis, EMG signals were waveform-rectified and notch-filtered to remove 60Hz electrical noise. Videos were synchronized with EEG/EMG data in Spike2 software.

Virally injected mice were recorded once at 8-10 weeks post-AAV injection, whereas PFF-injected mice were recorded at 3-, 6- and 9-months post-injection (mpi) to allow for longitudinal assessment of RBD-like behaviors over time. Mice were allowed to acclimatize in the recording enclosure for 3 days before sleep-wake behaviors were recorded over 24 hours for 2 consecutive days. On completion of the last day of recordings, mice were disconnected from recording cables then sacrificed for tissue collection, or singly housed until their next set of recordings.

2.7. Analysis of sleep-wake behaviors

In RBD patients, symptoms are most prominent in the early morning hours, when REM sleep quantities are greatest. In mice, REM sleep amounts are greatest between 14:00-17:00 (ZT 7-10). As such, we focused on our analysis of sleep-wake behaviors during this period. Vigilance states were manually classified into 5-second epochs based on standard criteria[28),29)] using a custom script in Spike2 (CED). Bouts of REM sleep waw identified based on low-amplitude, high-frequency EEG activity peaking in the theta frequency range, accompanied by minimal EMG tone with phasic muscle twitches. An Excel macro was used to quantify the number, length, and proportion of the recording interval spent in each vigilance state. To analyze cortical activity, we applied Fast-Fourier transform to EEG signals and performed power spectrum analysis to determine the relative EEG power expressed within each frequency band.

To assess whether mice developed RBD-like behaviors, we analyzed EMG activity during REM sleep. In human patients, RBD symptoms consist of increases in tonic, phasic, or both components of REM sleep muscle activity,[12),30),31)] with phasic motor events constituting the vast majority of movements in a typical RBD episode.[32),33)] In mice, spontaneous REM sleep is similarly composed of tonic and phasic motor components.[31),34)] Therefore, to assess RBD-like behaviors in mice, we developed a program based on our previously published methods for quantifying phasic and tonic muscle activity in REM sleep.[34)] To do this, we used the first 2.25s of REM sleep to set a 99.99th percentile of EMG activity for each episode. Phasic motor events

(muscle twitches) were defined as brief EMG activations longer than 5ms that exceeded the 99.99%ile amplitude threshold; tonic activity was equal to or below this threshold. The number and total duration of phasic motor events were quantified for every REM episode from each mouse. To account for variation in EMG electrode placement between mice, REM sleep muscle tone was normalized to the amplitude of the EMG during NREM episodes from the same animal. To examine the temporal profile of movements within individual REM episodes, we standardized episodes by length into 20 subdivisions and quantified movements that occurred in each subdivision along the REM episode.

2.8. Behavioral procedures

To evaluate the effects of α-synucleinopathy on motor, cognitive, and emotional behaviors, sham and αSyn PFF-injected mice were subjected to a behavioral test battery at 3, 6 and 12 mpi. All testing was conducted between 08:00 - 12:00 during the light phase. The test order was open field, accelerating Rotarod, gait analysis and grip strength.

2.8.1. Open field activity

Spontaneous locomotion and rearing activity were assessed in an open field arena. The Photobeam Activity System (San Diego Instruments) was used to acquire data. The clear Plexiglas arena (14 in. x 14 in. x 18 in.) is fitted with a scaffold of IR emitters and detectors to collect peripheral, center and vertical (rearing) beam breaks. After a 30-minute habituation to the testing room, a 10-minute trial began with a mouse placed in the center of the arena. All trials were recorded by high-definition camcorders. Digitally recorded trials were processed for automated analysis by ANYmaze software (Stoelting Co, Il) to obtain additional measures.

2.8.2. Accelerating Rotarod

The Rotarod (IITC San Diego Ca.) is a one-inch diameter, horizontal rod with a coarse surface, programmable to accelerate at different rates. As the rod accelerates, the mouse must adjust the cadence of its stride to remain on the rod. Three trials per day are performed over three consecutive days with the Rotarod accelerating from four to forty rpm in three hundred seconds.

There is a thirty-minute intertrial interval when the mouse rests in its home cage. On the very first trial, the mouse is habituated to the stationary rod for two minutes before rotation begins. A trial ends when the mouse fails to walk, by either falling from the rod or making a full rotation while gripping the rod. Mice that complete the full three hundred-second trial are removed from the rod to end the trial.

2.8.3. Catwalk XT gait analysis

The Catwalk XT (Noldus Information Technology, Netherlands) is a sophisticated system used to acquire quantitative measures of stride dynamics and paw placement. After a thirty-minute habituation to the darkened procedure room a trial is started by placing a mouse at one end of a forty cm enclosed alley. The mouse walks freely toward a goal box containing its home cage. Data is collected over a twenty cm sampling region. Footfalls are illuminated from below and pixelated to collected data on limb motion, stride dynamics and ambulation patterns. Additionally, the pixelated paw print data provides measures of load, braking, standing and propulsion during passive ambulation. The criteria for a compliant run were set to a duration of one half to ten seconds. At least five runs were collected for each mouse then post hoc visual validation of runs provided at least three runs for each mouse for analysis.

2.8.4. Grip strength

Grip strength meters are used routinely to assess strength as part of a general health assessment. After thirty minutes of habituation to the procedures room, a Grip Strength Meter (IITC Instruments, San Diego, Ca) is used to measure forepaw and hindpaw grip strength on subsequent days. For forepaw, a mouse is lowered by the tail so that it grasps a metal T bar with forepaws only. The mouse is pulled backward slowly by the tail in the horizontal plane to exert a force on the T bar, which is transduced to a meter that records the maximum force (grams) exerted before the release of the bar. Five trials are performed with a twenty-minute intertrial interval. Twenty-four hours after the forepaw trails, hindpaw grip strength is measured. For hindpaw the T bar is replaced with a chicken wire grid. A mouse is lowered so that it grasps the grid with all four paws. Similar to the forepaw test, the mouse is slowly pulled backward in the horizontal plane to exert a

force on the T bar which is transduced to a meter that records the maximum force (grams) exerted before the release of the bar. Five trials are performed with a twenty-minute intertrial interval.

2.9. Tissue preparation

For pathological analysis, αSyn PFF-injected mice were sacrificed at 1, 3, 6, 12 mpi and immunohistochemical analysis was performed using formalin-fixed paraffine-embedded tissue. Mice that underwent electrophysiological study till 9-month post-injection (mpi) were sacrificed after completion of electrophysiological experiments and immunohistochemical analysis was performed using fresh frozen tissue.

2.9.1. Formalin-fixed paraffine-embedded tissue

Mouse brains were perfused intracardially with 15mL of phosphate buffered saline (PBS) and 15ml of 4% (w/v) paraformaldehyde in PBS and fixed in 4% (w/v) paraformaldehyde in PBS at 4°C overnight. The brains were embedded in paraffin and then sectioned with a thickness of 6μm using a microtome and mounted on glass slides. For immunohistochemical analyses, the sections were incubated at 4°C for 2 days with following primary antibodies: an anti-p-αSyn antibody EP1536Y (Abcam #ab51253, 1:10,000). For generating diaminobenzidine reaction product, biotinylated secondary antibodies (Vector laboratories #BA-2000, #BA-1000, #BA4000, 1:1000) were used and nuclei were counterstained with hematoxylin.

For immunofluorescence, the sections were incubated at 4°C for 2 days with the following primary antibodies: an anti-p-αSyn antibody EP1536Y (Abcam #ab51253, 1:10,000), an anti-TH antibody (Sigma-Aldrich #T2928, 1:5,000), an anti-ChAT antibody (Millipore #AB144P, 1:200), an anti-NeuN antibody (Millipore #MAB377, 1:200), an anti-GFAP antibody (Covance #SMI-21R, 1:1,000), an anti-Iba1 antibody (Thermo-Fisher Invitrogen #MA5-27726, 1:100), and an anti-SOX10 antibody (R&D Systems #AF2864, 1:3000). Fluorescent dye-conjugated secondary antibodies (Thermo-Fisher #A11055, #A21202, #A21207, #A31573, 1:500) were used, and nuclei were stained with DAPI. Sections were examined with an Eclipse Ni microscope (Nikon) or using a Lamina Scanner (PerkinElmer; 20 × objective).

2.9.2. Fresh frozen tissue

Upon completion of behavioral experiments, mice were deeply anesthetized, transcardially perfused with PBS followed by 4% paraformaldehyde and their brains harvested. Following fixation, brains were cryoprotected with 30% sucrose, frozen in Tissue-Tek O.C.T. compound (Sakura) and cut into 30μm-thick coronal sections.

2.10. Immunohistochemical analysis

For formalin-fixed paraffine-embedded human and mouse tissue, the sections were incubated at 4°C for 2 days with the following primary antibodies: an anti-p-αSyn antibody EP1536Y (Abcam #ab51253, 1:10,000), an anti-TH antibody (Sigma-Aldrich #T2928, 1:5,000), an anti-ChAT antibody (Millipore #AB144P, 1:200), an anti-GFAP antibody (Covance #SMI-21R, 1:1,000), an anti-Iba1 antibody (Thermo-Fisher Invitrogen #MA5-27726, 1:100), and an anti-SOX10 antibody (R&D Systems #AF2864, 1:3000). Fluorescent dye-conjugated secondary antibodies (Thermo-Fisher #A11055, #A21202, #A21207, #A31573, 1:500) were used, and nuclei were stained with DAPI. Sections were examined with an Eclipse Ni microscope (Nikon) or using a Lamina Scanner (PerkinElmer; 20 × objective).

For fresh frozen tissue, immunohistochemistry was performed on free-floating brain sections as previously described.[21)] Sections were washed, blocked in 4% goat serum for 1 hour, then incubated in primary antibodies for up to 48 hours at 4°C. For visualization, sections were incubated in fluorophore-conjugated secondary antibodies for 1 hour at room temperature, counterstained with DAPI, and mounted on glass slides.

RNA-based in-situ hybridization was used to characterize the molecular identity of pathologically affected SLD neurons. Mouse brains were collected as described above, cut into 16μm-thick sections, then mounted on glass slides. The RNAscope multiplex fluorescent reagent version 2 assay (RNAscope, Advanced Cell Diagnostics) was conducted on brain sections according to manufacturer protocol, as described elsewhere. Target retrieval reagent and protease were sequentially added to slides, followed by application of the target probe for Slc17a6 (VGLUT2) and Slc32a1 (VGAT) mRNA transcripts. The signal was then amplified with multiplex

fluorescent v2 AMP1 solution then visualized with Cy3 fluorescent dye. To stain for αSyn aggregates, pSyn immunostaining was performed after the RNAscope protocol on slide-mounted.

Both upright (Zeiss AxioImager.Z1) or confocal (Zeiss LSM 900 or Leica TCS SP8) microscopes were used to acquire images of immunofluorescent signals. All quantitative image analyses were performed at three rostral-caudal positions of the SLD. The same approach was used to quantify immunofluorescent signals in experimental and control animals. During image analysis, automated errors were corrected by an experienced observer to ensure that image artifacts were not included.

2.11. Automated quantification of αSyn pathology

Scanned whole-slide images were imported into QuPath to generate two subsets of images in PNG format compatible with a workflow modified from QUINT:[35] "registration" images (low-resolution full-color PNGs for Allen Brain Atlas registration) and "segmentation" images (full-resolution binary PNGs containing only pathology-positive pixels). Registration images were given to DeepSlice,[36] then manually adjusted for increased accuracy. This output was run through the "quantifier" function in NUTIL to generate a regional breakdown of each image.[37] Images where 30% or more of the total area contained ROIs were considered relevant for further processing and the corresponding segmentation images were manually filtered for artifacts in GIMP, which primarily consisted of non-specific edge staining. Filtered segmentation images were then fed back into the NUTIL quantifier function to generate a pathology pixel count for each brain region. An R script was created to compile the data for each brain across the study, calculate load metrics (pathologic area/total region area,) and to filter out irrelevant regions. Where noted, sub-regions defined by the ABA were combined into their parent features. Resultant data was used to generate heatmaps in GraphPad Prism (version 10).

2.12. Statistical analysis

Results for all statistical tests are described in the figure captions. Statistical analysis of data and graphing was performed in Graphpad Prism version 9.00 (GraphPad Software) and R software, v.4.2.1 (R Foundation for Statistical Computing, R-project.org/). For all tests, a critical value of α

$\leq$ 0.05 was set. Outliers were assessed using the ROUT method[38] with a false discovery rate of 1% used as the exclusion criteria. The Kolmogorov-Smirnov test was used to examine the normality of the distribution of variables. To compare longitudinal data between two groups, we used a two-way repeated measures ANOVA for parametric variables and Brunner & Langer test for non-parametric variables, with Tukey post-hoc comparisons, where applicable.

III. RESULTS

3.1. RBD patients exhibited αSyn pathology within the SLD

A rich history of animal studies has established the SLD as the physiologic substrate for muscle suppression during REM sleep, highlighting its dysfunction as the pathophysiologic substrate for RBD in humans. Although αSyn pathology has been observed in brainstem areas encompassing the SLD in isolated RBD cases and in cases with comorbid PD,[13),14)] the extent of anatomical overlap with this region in humans and its homolog in animals remains unclear. To root our animal experiments in clinical relevance, we conducted histopathological analysis on brain tissue from patients with PD with or without comorbid RBD, as well as on brains from healthy elderly individuals. Immunohistochemical staining for phosphorylated αSyn (p-αSyn), a specific marker for pathological forms of αSyn, revealed numerous αSyn aggregates in the SLD of PD patients with comorbid RBD, whereas aggregates were sparse or absent in PD patients without RBD and healthy controls, respectively (Figs 1A-C). Quantification confirmed that patients with RBD had higher p-αSyn immunoreactivity in the SLD compared to controls, which suggests that αSyn pathology in the SLD is correlated with the expression of RBD in humans (Fig 1D).

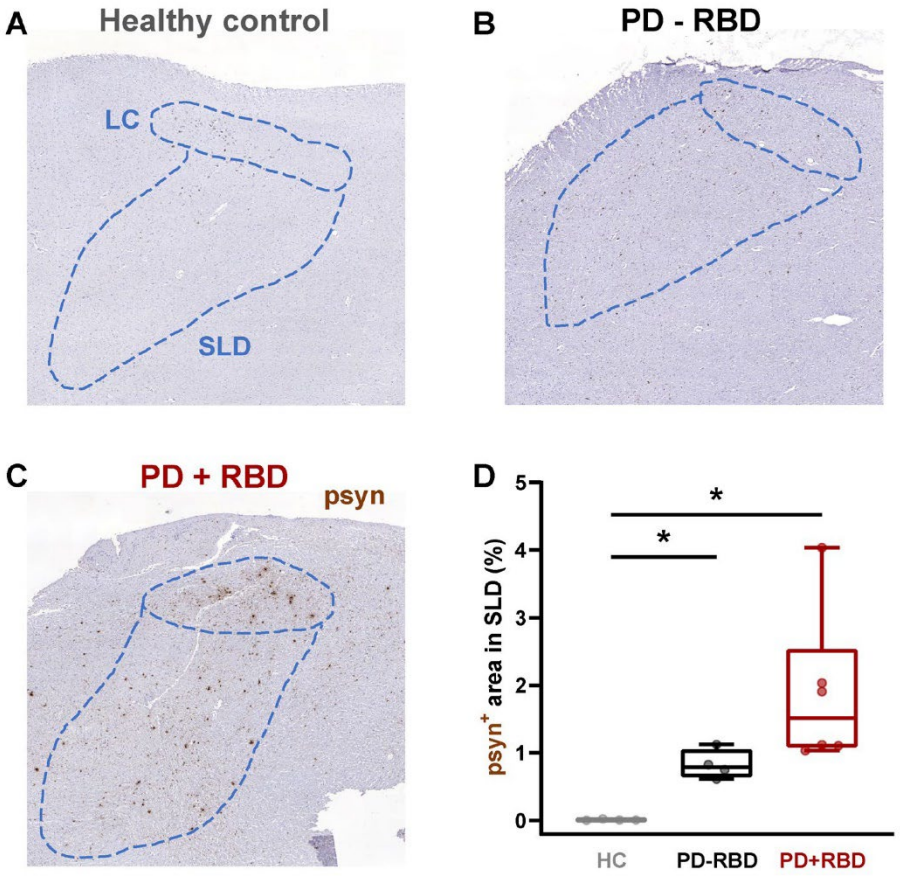

Fig 1. Pathological αSyn accumulation in the SLD was associated with RBD in human patients. DAB staining for phosphorylated αSyn (p-αSyn, depicted in brown) was conducted on post-mortem brain samples from three groups: **A)** healthy elderly individuals, **B)** Parkinson's disease patients without RBD diagnosis (PD-RBD), and **C)** Parkinson's disease patients with RBD (PD+RBD). The pontine regions, specifically the locus coeruleus (LC) and SLD, are marked in blue. The results indicate a notable presence of αSyn aggregates in the SLD of patients with RBD when compared to both PD patients without RBD and healthy controls. **D)** Quantitative analysis of pathological αSyn burden in the SLD shows a gradient of pathology from healthy controls to the PD-RBD and PD+RBD groups. While the PD-RBD group typically showed fewer αSyn aggregates than the PD+RBD group, they still presented with a significantly higher number of αSyn aggregates compared to healthy controls.

3.2. AAV-driven overexpression of αSyn in SLD neurons induced RBD-like behaviors in mice

Previous animal models of RBD have largely consisted of lesion or loss of function manipulations of the SLD[24),25),39),40)] which do not reflect the pathologic basis of PD. On the other hand, while recent models involve the induction of widespread αSyn pathology across various brain regions,[41),42)] they do not allow for effective isolation of RBD symptomatology to specific changes in the SLD. These limitations in modeling RBD complicate the identification of a direct causal relationship between SLD dysfunction and RBD symptoms, leaving uncertainties regarding the specific SLD cell types directly involved in the disorder.

Having shown that SLD pathology is correlated with RBD in humans, we sought to establish this relationship causally by inducing αSyn pathology in the SLD of mice then determining whether they developed RBD-like behaviors. To this end, we injected mice with an AAV vector to drive the overexpression of αSyn in SLD neurons. This intervention resulted in robust transduction of αSyn within SLD neurons (Fig 2A), confirming that we effectively targeted the SLD. Since human RBD is marked by elevated tonic and/or phasic EMG activity during REM sleep,[12),30),31)] we assessed whether mice presented with an RBD-like phenotype by quantifying tonic and phasic components of REM sleep motor activity at 8-10 weeks post-viral injection. We found that the targeted overexpression of αSyn in SLD neurons increased the number and total duration of phasic motor events during REM sleep, which denotes elevated motor activity during REM sleep (Figs 2B-E). Despite motor hyperactivity during REM sleep, other component phenomena such as EEG activity, or the state of REM sleep itself were unaffected by αSyn overexpression (Figs 2F-G). Together, these findings therefore highlight a specific role for SLD neurons in REM sleep motor suppression.

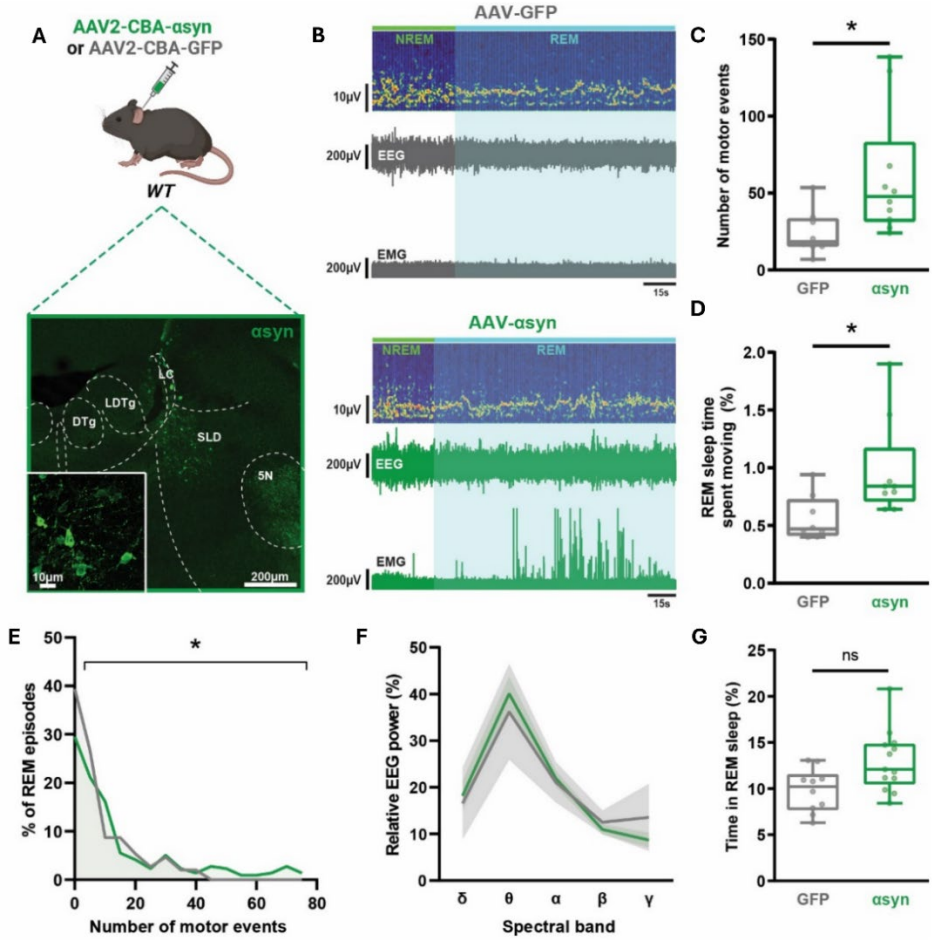

Fig 2. Viral overexpression of αSyn in SLD neurons was associated with elevated muscle activity during REM sleep. A) The experimental design is illustrated schematically, accompanied by a representative image demonstrating immunofluorescent labeling of αSyn in SLD neurons (green) taken eight weeks after AAV inoculation. **B)** Shown are simple electrophysiological recordings from mice that received AAV-GFP (grey) or AAV-αSyn (green) eight weeks post-injection. It is notable that the αSyn-transduced mouse exhibited increased EMG activity during REM sleep (cyan). **C)** Analysis of EMG activity indicates that the AAV-αSyn injection resulted in a higher frequency of motor events during REM sleep (*$P < 0.05$), and **D)** a greater proportion of REM sleep time was characterized by movements (*$P < 0.05$). **E)** The frequency distribution of REM sleep episodes was assessed for both AAV-αSyn injected mice and controls, with the former exhibiting a tendency towards REM sleep episodes marked by increased movements compared to the control group (*$P < 0.05$). **F, G)** There were no significant differences in EEG cortical activity during REM sleep or overall amounts of REM sleep between AAV-αSyn injected mice and GFP-injected controls ($P > 0.05$).

3.3. PFF inoculation into the SLD initiated propagative αSyn pathology in the mouse brain

We have shown that αSyn pathology causes RBD symptoms when it is localized to the SLD. Unlike the stationary pathology featured in viral vector models however, synucleinopathy propagates throughout the brains in human patients, a phenomenon that has been modeled extensively in animal models.[23),42)] It is precisely this pathological process that we propose drives phenoconversion from RBD to fulminant PD. To test this hypothesis, we injected αSyn PFFs into the SLD to initiate propagative synucleinopathy from the SLD of wild-type mice (Fig 3). Then, we conducted histopathologic, electrophysiological and behavioral assessments till 9-12 mpi to longitudinally track the propagation of αSyn pathology in the mouse brain and subsequent development of RBD-like phenomena and Parkinsonian motor deficits.

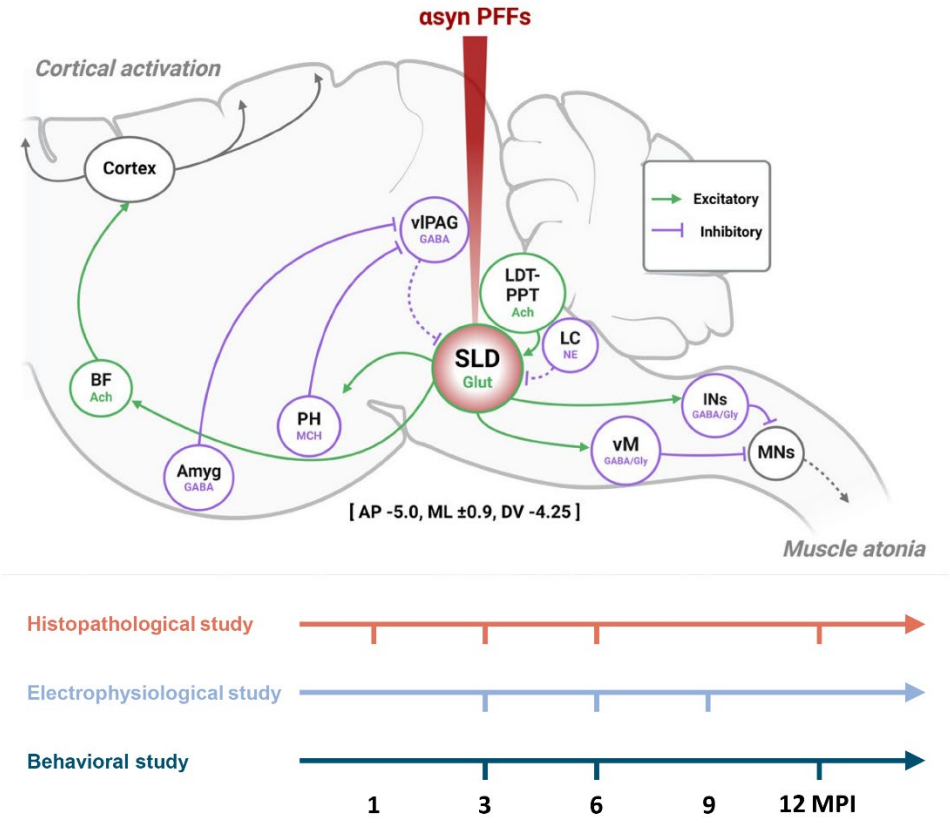

Fig 3. Experiment schematic of αSyn PFF injection into the SLD. Schematic map shows neural circuit of cortical activation and muscle atonia during REM sleep. αSyn PFF was injected into the SLD, the main neural correlate of REM sleep. The mice for histopathologic analysis were aged 1, 3, 6, or 12 mpi and assessed for the spreading of p-αSyn pathology during that time. The mice for electrophysiological analysis were aged till 9 mpi and conducted sleep-wake recording at 3, 6, and 9 mpi. The mice for behavior analysis were aged till 12 mpi and underwent motor battery at 3, 6, and 12 mpi. **Abbreviations** = Ach, acetylcholine; AP, anteroposterior; BF, basal forebrain; DV, dorsoventral; Glut, glutamate; Gly, glycine; INs, motor neurons in the spinal cord; LC, locus coeruleus; LDT, laterodorsal tegmental nucleus; MCH, melanin concentrating hormone; ML, mediolateral; MNs, motor neurons in the spinal cord; NE, norepinephrine; PH, posterior hypothalamus; PPN, pedunculopontine nucleus; SLD, sublaterodorsal tegmental nucleus; vlPAG, ventrolateral periaqueductal gray; vM, ventral medial medulla.

First, we found that αSyn PFF injection induced the formation of αSyn aggregates in SLD neurons from 1 mpi, which were labeled by p-αSyn immunostaining (Figs 4A–B). This pathology propagated throughout the brains of PFF-injected mice over time, resulting in αSyn aggregation in distant brain regions by 12 mpi (Figs 4C–D). A heatmap and representative DAB images showed that at 1 mpi, αSyn aggregates propagated to nearby pontine structures including the laterodorsal tegmental nucleus, pedunculopontine nucleus, and parabrachial nucleus, to the periaqueductal grey in the midbrain, and to ventral medial medullary structures including magnocellular reticular nucleus and paragigantocellular reticular nucleus which are important for the generation of REM sleep atonia. At 3 mpi, pathologies propagated further caudally to the cervical spinal cord and rostrally to midbrain reticular nucleus, central amygdalar nucleus, bed nuclei of the stria terminalis, and dorsal part of endopiriform nucleus. At 6 mpi, αSyn neuronal pathologies were found in the substantia nigra pars compacta and ventral tegmental area. Also, they were found in hypothalamic structures including medial mammillary nucleus and lateral hypothalamic area, nucleus accumbens, infralimbic area, and taenia tecta. Till 12 mpi, pathologies went further to some hypothalamic structures including the tuberomammillary nucleus and medial preoptic area and cortical structures including the anterior cingulate area and auditory areas.

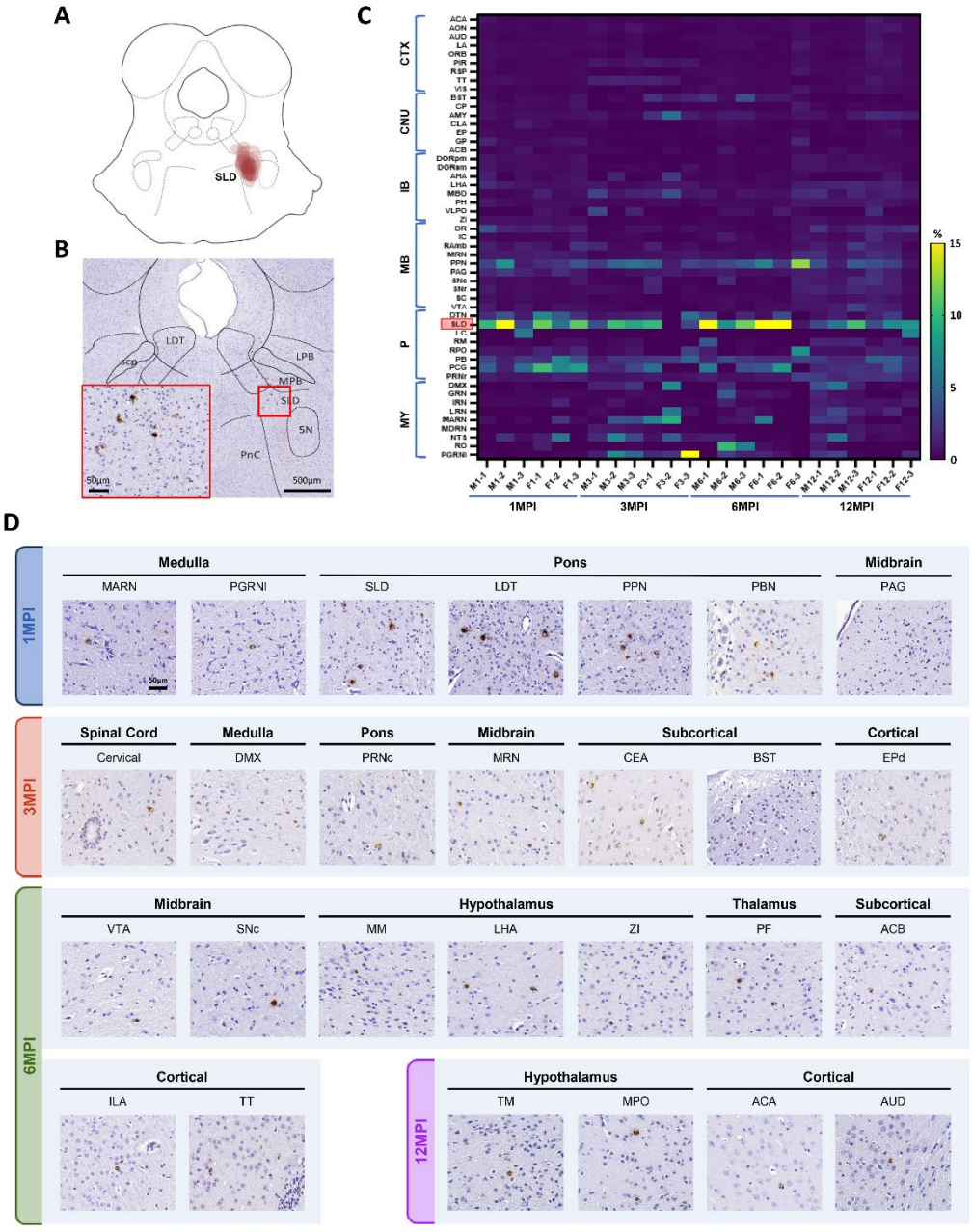

Fig 4. Propagation of α pathology from the SLD injected with αSyn PFFs. A) Injection of wild-type mouse αSyn into the right SLD of wild-type mice. **B)** Representative DAB staining showing the presence of endogenous αSyn pathology in the SLD at 1 mpi. **C)** Heatmap shows the burden of pathological αSyn aggregates in each brain region which was quantified by automatic quantification.

Pathological burden was defined as the ratio of p-αSyn positive area to the total area across each region. The brain regions were arranged along the y-axis, starting from medulla oblongata (bottom) to the cortical region (top). The x-axis displays data from a total of 24 mice, ranging from 1 mpi (left) to 12 mpi (right). A red box highlights the injection site, the SLD. **D)** Representative images of p-αSyn DAB staining in brain lesions from 1 mpi to 12 mpi. **Abbreviations** = ACA, anterior cingulate area; ACB, nucleus accumbens; AHA, anterior hypothalamic area; AMY, amygdala; AON, anterior olfactory nucleus; AUD, auditory area; BST, bed nuclei of the stria terminalis; CLA, claustrum, CNU, cerebral nuclei; CP, caudoputamen; CTX, cerebral cortex; DMX, dorsal motor nucleus of the vagus nerve; DORpm, polymodal association cortex related thalamus; DORsm, sensory-motor cortex related thalamus; DR, dorsal nucleus raphe; DTN, dorsal tegmental nucleus; EP, endopiriform nucleus; F, female; GP, globus pallidus; GRN, gigantocellular reticular nucleus; IB, interbrain; IC, inferior colliculus; ILA, infralimbic area; IRN, intermediate reticular nucleus; LA, limbic area; LC, locus coeruleus; LHA, lateral hypothalamic area; LPB, lateral parabrachial nucleus; LRN, lateral reticular nucleus; M, male; MARN, magnocellular reticular nucleus; MB, midbrain; MBO, mammillary body; MDRN, medullary reticular nucleus; MM, medial mammillary nucleus; MPB, medial parabrachial nucleus; MPO, medial preoptic area; MRN, midbrain reticular nucleus; MY, medulla; NTS, nucleus of the solitary tract; ORB, orbital area; P, pons; PAG, periaqueductal gray; PB, parabrachial nucleus; PCG, pontine central gray; PF, parafascicular nucleus; PGRNl, lateral part of the paragigantocellular reticular nucleus; PH, posterior hypothalamic nucleus; PIR, piriform area; PnC, caudal part of the pontine reticular nucleus; PPN, pedunculopontine nucleus; PRNr, pontine reticular nucleus; RAmb, midbrain raphe nuclei; RM, raphe magnus; RO, nucleus raphe obscurus; RPO, nucleus raphe pontis; RSP, retrosplenial area; SC, superior colliculus; SCP, superior cerebellar peduncle; SLD, sublaterodorsal tegmental nucleus; SNc, compact part of the substantia nigra; SNr, reticular part of the substantia nigra; TM, tuberomammillary nucleus; TT, taenia tecta; VIS, visual area; VLPO, ventrolateral preoptic nucleus; VTA, ventral tegmental area; ZI, zona incerta; 5N, motor trigeminal nucleus.

Second, we characterized the SLD cell types susceptible to PFF-induced αSyn pathology and those involved in RBD pathogenesis. Among neuronal cell, most p-αSyn pathologies were co-localized with ChAT+ neurons, but not with other neuronal markers including TH+, vglu2+ encoding mRNA transcript, and vgat encoding mRNA transcript at 6 mpi in the SLD (Fig 5A–D). Among glial cell, most p-αSyn pathologies were co-localized with SOX10+ cells, but not with GFAP+ and IBA1+ cells (Fig 5E–G). Then, we calculated the percentage of p-αSyn pathology in NeuN+, ChAT+, and SOX10+ cells among total p-αSyn pathology. Till 3 mpi, almost all p-αSyn pathologies were in neurons, and from 6 mpi, the percentage gradually decreased (Fig 5H). Most of the neuronal p-αSyn pathologies belonged to cholinergic neurons (Fig 5I). Instead, p-αSyn pathologies started to aggregate in SOX10+ cell from 6 mpi (Fig 5J).

Finally, given that PD symptomatology is thought to reflect αSyn-associated neuronal loss rather than αSyn aggregation per se, we asked whether PFF injection caused overt degeneration in the mouse SLD. To answer this question, we performed immunohistochemistry on brain sections for the neuronal marker NeuN then quantified the number of remaining SLD neurons in PFF-injected mice. We found that PFF injection caused a 23% reduction in the number of SLD neurons by 9 mpi relative to PBS controls, which suggests that αSyn aggregation led to significant neuronal loss in the SLD (Figs 5K-O).

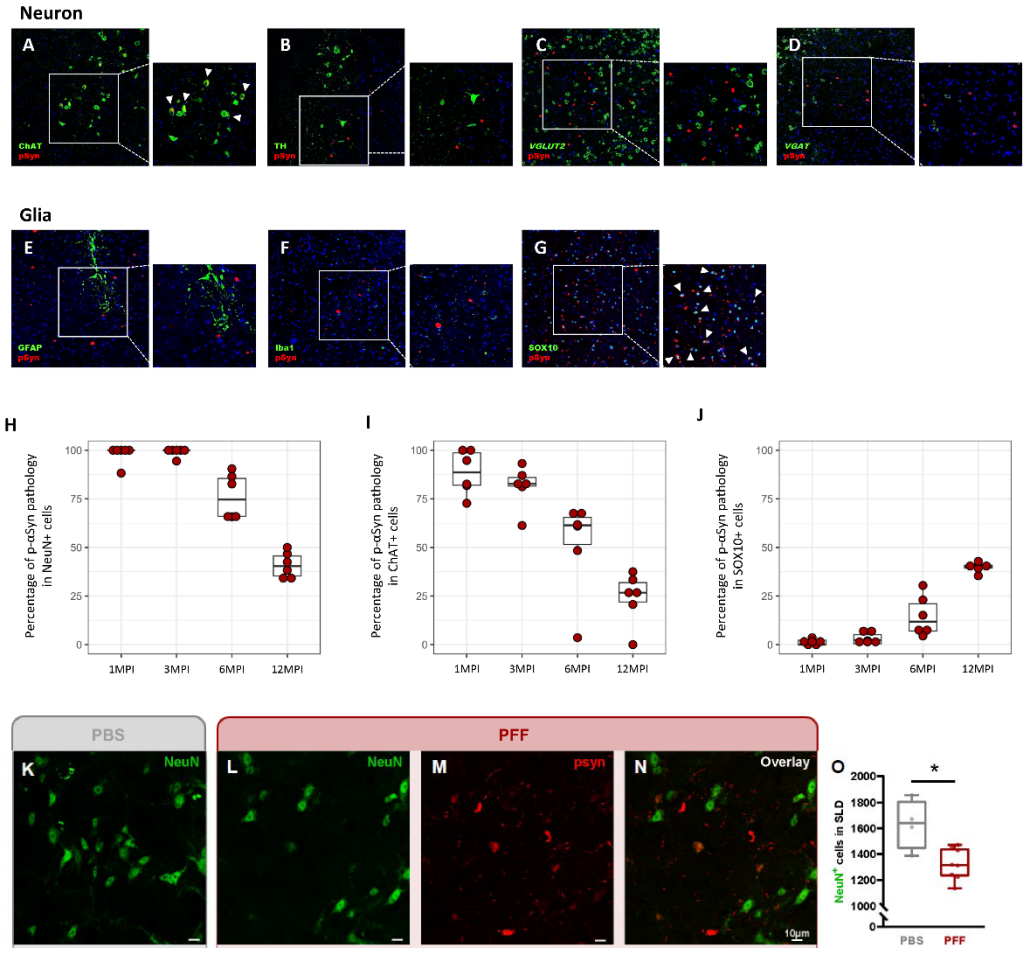

Fig 5. Subcellular population in the SLD vulnerable to αSyn pathology. A) Immunofluorescence staining images show the colocalization of p-αSyn (red) and ChAT (green) in the SLD (arrowheads) in a mouse injected with αSyn PFF at 6 mpi. **B-D)** Micrographs show no colocalization of p-αSyn (red) and neuronal markers (green), such as TH, vGLUT2 mRNA, and vGAT mRNA. **E-F)** Micrographs show immunostaining for p-αSyn (red) and glial markers (green), such as GFAP, Iba1, and SOX10. p-αSyn aggregates were not colocalized with GFAP- and Iba1-positive cells, but with Sox10-positive cells. **H-J)** The majority of p-αSyn-positive signals were colocalized with neurons, particularly cholinergic neurons, till 3 mpi. From 6 mpi, there was a notable decrease in the proportion of p-αSyn+ aggregates in cholinergic neurons, coupled with a gradual increase in oligodendrocytes. **K)** Immunofluorescence staining images show NeuN (green) and p-αSyn (red) in the SLD in a PBS-injected mouse, compared to **L-N)** a PFF-injected mouse. **O)** Quantitative assessment of NeuN-positive cells in the SLD indicated a significantly lower number of neurons in the SLD in PFF-injected mice (red) than those in controls (gray) at 9 mpi.

3.4. Seeded αSyn pathology in the SLD was associated with RBD-like behaviors in mice

Having demonstrated that PFF injection triggers propagative αSyn pathology from the SLD and that targeted SLD pathology elicits RBD-like behaviors, we next investigated whether propagation beyond the SLD would advance PD past its prodromal stage (RBD). After injecting recombinant αSyn PFFs into the SLD of wild-type mice, RBD-like behaviors were evaluated based on EMG measurements and video footage collected from 3-9 mpi. Importantly, we found that pathological seeding in the SLD was associated with an RBD-like phenotype as early as 3 mpi. Specifically, PFF-injected mice had heightened muscle activity during REM sleep, as exemplified by increases in the number of phasic motor events (Figs 6A-B), the time these events occupied in REM sleep bouts (Fig 6C), as well as more variable muscle tone during REM sleep (Fig 6D).

In human patients, the expression of RBD symptoms differs from night to night, as well as within a single night of sleep.[43] Given this, we evaluated whether PFF-inoculated mice accurately reflected such temporal variations in RBD symptoms by analyzing the distribution of movements across and within individual bouts of REM sleep. Consistent with the overall increase in REM sleep movements, we found that PFF injection shifted the distribution of REM sleep episodes such that PFF-injected mice had a higher proportion of REM episodes containing more motor events, which denotes a propensity for REM sleep with more movement (Fig 6E). In addition, we observed marked differences between groups in the patterns of motor activity within individual REM sleep episodes. Motor events were elevated throughout the duration of REM sleep bouts in PFF-injected mice compared to controls. (Figs 6F-G) Therefore, our findings demonstrate that PFF injection affects the coordination of motor suppression both within and across REM sleep episodes in a manner that mimics the symptomatic profile of RBD patients.

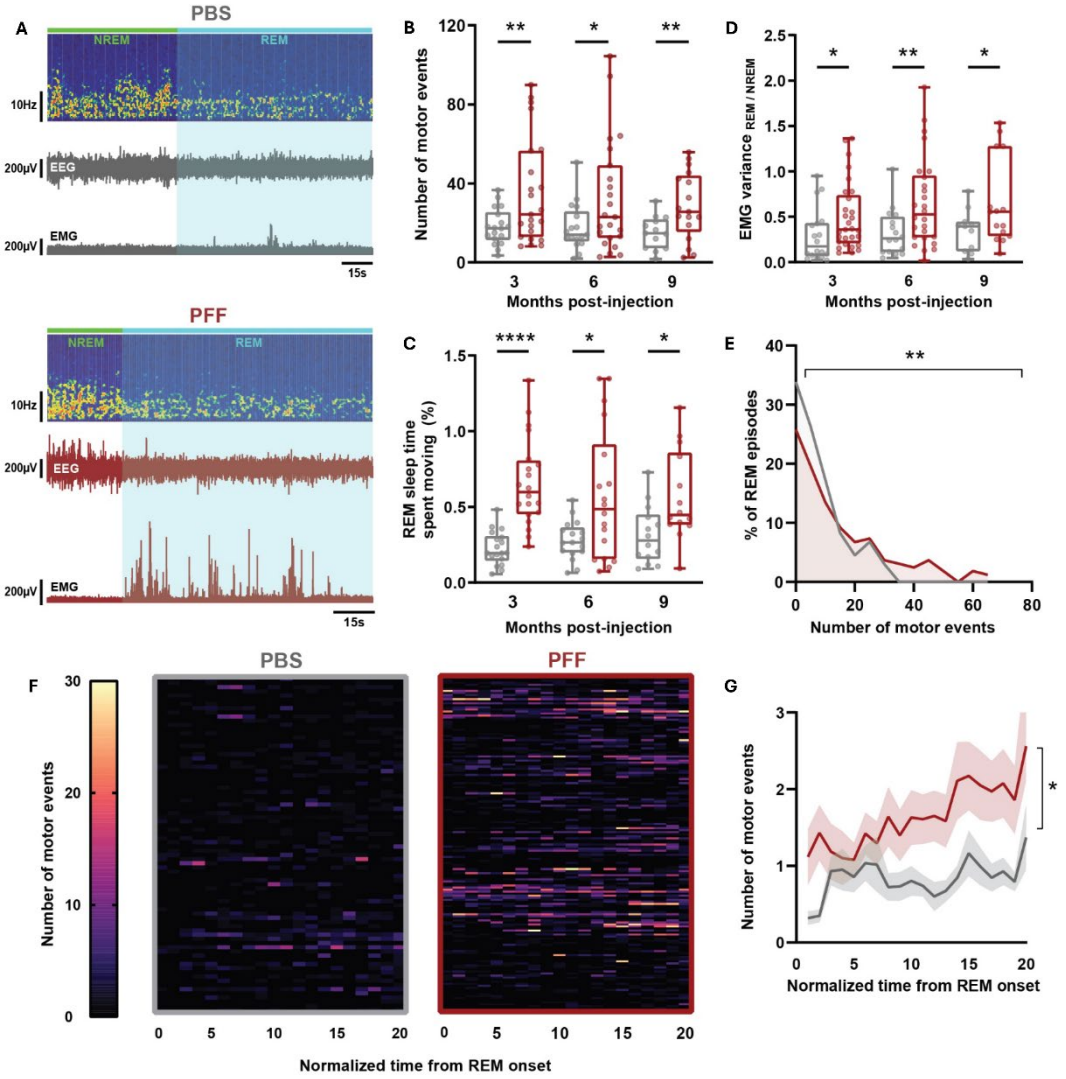

Fig 6. aSyn PFF inoculation into the SLD led increased muscle activity during REM sleep. A) An example electrophysiological trace from a mouse injected with αSyn PFF (red) in the SLD at 9 mpi and PBS control (grey). The PFF-injected mouse exhibited pronounced muscle activity during REM sleep (cyan). **B)** Quantitative analysis of EMG activity indicates increased number of motor events during REM sleep (*$P < 0.05$, **$P < 0.01$) and **C)** the REM sleep time spent moving between at 3, 6, and 9 mpi (*$P < 0.05$, ****$P < 0.0001$). **D)** The ratio of variance in EMG activity between REM and NREM sleep was greater in PFF-injected mice compared to control mice (*$P < 0.05$, **$P < 0.01$). **E)** The PFF-injected mice showed a significantly higher proportion of REM episodes that had increased number of motor events compared to the control group at 6 mpi (**$P < 0.01$). **F)** Heatmap representations display EMG activity across all REM sleep episodes for the PBS (left) and

PFF-injected mice (right) at 6 mpi, with all REM sleep bouts standardized in length. The PFF group showed a tendency of increased motor events across all REM episodes. **G)** The comparison of the number of motor events within individual REM sleep episodes from PFF-injected mice (red) and PBS controls (grey), showing more frequent movements across the entire REM sleep bouts (*****$P < 0.05$).

3.5. PFF-injected mice displayed cortical EEG slowing and perturbed sleep-wake architecture

Despite RBD being the most prominent sleep disturbance in early-stage PD, patients frequently experience impaired cortical activation along with additional sleep issues such as insomnia and sleep fragmentation particularly at later stages of disease[44),45)] These observations suggest that transmissible αSyn pathology contributes to the progressive disruption of sleep-wake physiology throughout the course of PD. To evaluate the impact of PFF injection on cortical activation, we conducted spectral analysis of EEG activity across different vigilance states. From 6 mpi, PFF-injected mice exhibited a shift in their EEG spectra to lower frequencies, consisting of reduced theta power and increased delta power during NREM sleep, REM sleep and wakefulness (Figs 7A-C). This generalized slowing of the EEG was also reflected by a consistent reduction in the ratio of power between theta and delta frequencies across all vigilance states (Fig 7D). Moreover, PFF injection led to increased wakefulness and reduced NREM and REM sleep quantities from 6 mpi (Figs 7E-G). This sleep loss appeared to derive from wake consolidation in PFF-injected mice, with less frequent but prolonged wake bouts (Fig 7H). Altogether, these data demonstrate that PFF inoculation induced broader sleep disturbances reminiscent of cortical EEG slowing and sleep loss in human PD.

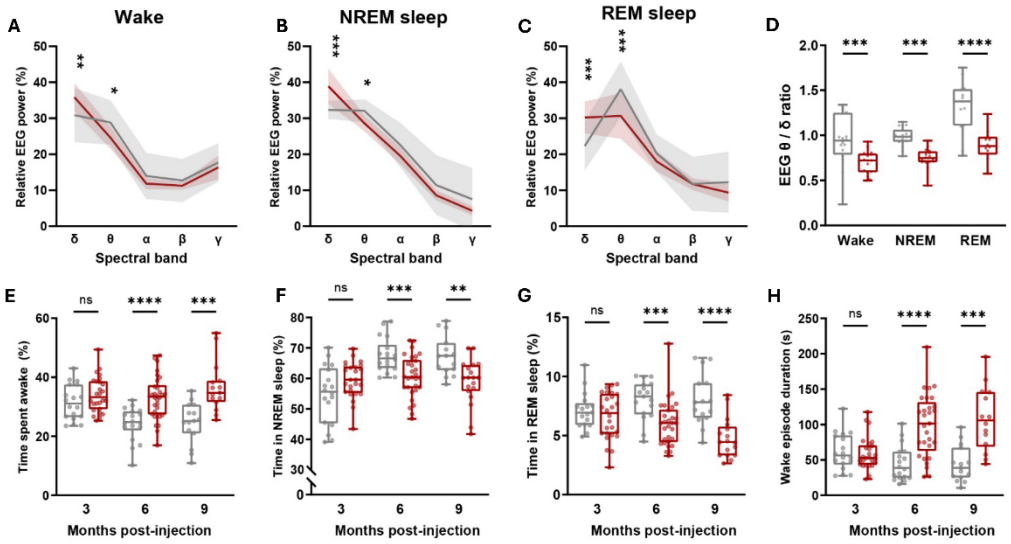

Fig 7. Cortical slowing and increased awakening after the initial RBD-like behaviors. A) The EEG power spectrum distribution is presented for PFF-injected mice (red) and PBS controls (grey) at 6 mpi during wakefulness, **B)** NREM sleep, and **C)** REM sleep (*$P < 0.05$, **$P < 0.01$, ***$P < 0.001$). Notably, PFF-injected mice exhibited a significantly lower proportion of theta power and higher proportion of delta power across all states. **D)** The theta-to-delta power ratio was significantly reduced across all sleep-wake states at 6 mpi (***$P < 0.001$, ****$P < 0.0001$). **E)** PFF-injected mice allocated more time to wakefulness and less time to **F)** NREM and **G)** REM sleep at 6 and 9 mpi (**$P < 0.01$, ***$P < 0.001$, ****$P < 0.0001$). **H)** The observed alterations in the PFF group are likely attributed to prolonged wake episodes at 6 and 9 mpi (***$P < 0.001$, ****$P < 0.0001$).

3.6. Propagative αSyn pathology precipitated Parkinsonian motor deficits in mice

Previous PFF inoculations in rodents have demonstrated that multiple routes of pathologic propagation converging on the midbrain nigrostriatal circuit can each lead to the onset of PD-like motor deficits.[23),24)] In humans, αSyn pathology associated with RBD is thought to give rise to clinical PD when it reaches and leads to neuronal loss in the substantia nigra pars compacta.[11),46)] Given our findings that seeded αSyn pathology in the SLD results in RBD-like symptoms, as well as its subsequent propagation from the SLD to the substantia nigra pars compacta, we next aimed to determine if PFF-injected mice that initially developed RBD would progress into to a manifest, Parkinsonian phenotype.

To assess waking motor function of PFF-injected mice, we used a battery of motor tests including open field, rotarod, grip strength testing and catwalk gait analysis. Analysis of various gait parameters revealed that PFF-injected mice developed prolonged swing speed and contact time of both forepaw and hindpaw at 12 mpi (Fig 8A). When analyzed by sex, significant differences were observed only in male mice. Mice inoculated with PFFs did not differ in activity in open field, grip strength, or rotarod performance at the timepoints examined in our study (Figs 8B–D). Our findings demonstrate that PFF-injected mice presented with a clear, clinically relevant motor signature reminiscent of gait deficits seen in human PD.[47)]

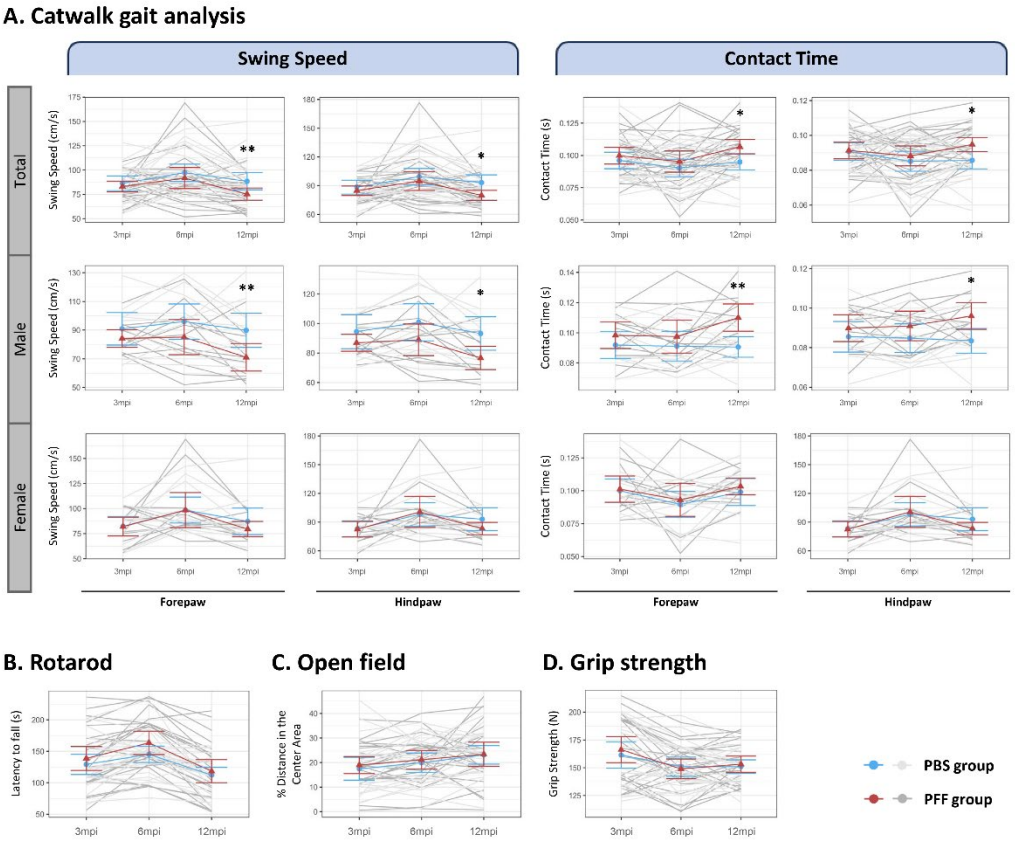

Fig 8. αSyn PFF injection into the SLD led to the development of gait dysfunction. A) The CatWalk XT was conducted to evaluate automated, multiparametric mouse locomotion. Mice injected with αSyn PFF exhibited prolonged swing speed and increased contact time at 12 mpi compared to those injected with PBS (*$P < 0.05$, ** $P < 0.01$). The analyses were also conducted separately based on sex. **B-D)** No significant differences were observed in latency time to fall during the Rotarod test, the percentage of distance traveled in the center area during the open field test, or grip strength when comparing PFF-injected mice to PBS-injected controls.

IV. DISCUSSION

Synucleinopathies are increasingly understood through the lens of αSyn pathology, rather than purely symptomatic definitions.[48),49)] Despite the substantial body of evidence qualifying RBD as a synucleinopathy, a fundamental gap remains in understanding its mechanisms. The present study offers a detailed characterization of a mouse model of α-synucleinopathy that mirrors pathological and symptomatic features of PD. Notably, we demonstrate that PFF injection initiated synucleinopathy in the SLD, which precipitated the onset of RBD-like behaviors in mice. Considerable phenotypic variation exists across different animal models of RBD, with earlier SLD loss of function manipulations showing changes in phasic muscle activity during REM sleep,[40),50),51)] whereas recent synucleinopathy-centered models report changes in the intensity or variance of muscle tone.[24),41)] According to current diagnostic criteria, RBD in humans is characterized by phasic and/or tonic muscle hyperactivity in REM sleep.[52)] Our results thus reconcile a discrepancy between animal models and human patients, as PFF-inoculated mice had more variable tone in addition to phasic motor excesses during REM sleep. On top of the fact that intermittent motor behaviors are more frequent than sustained events in RBD episodes,[33)] phasic, but not tonic increases in EMG activity were recently shown to distinguish between subsets of PD patients with or without RBD from healthy controls.[51)] Phasic RBD metrics also correlated with measures of magnetic susceptibility in the SN among RBD patients, but this was not observed for tonic parameters,[53)] illustrating the relationship of specific RBD symptoms with brain pathology. Hence, replicating this important and ubiquitous feature of human RBD is of great interest for developing clinically relevant animal models. Overall, our study affirms the role of SLD pathology in RBD and enhances our understanding of early disease mechanisms in prodromal PD.

To evaluate if the temporal dynamics of αSyn pathology corresponds with time-dependent changes in behavior, we assessed the progression of pathology in PFF-injected mice. Histological assessments revealed that αSyn aggregates were initially sparse in the SLD, then increased in abundance from 3-6 mpi. By 9 mpi, the numbers of aggregate-bearing SLD neurons decreased, which can be ascribed to cell loss. Unlike the SLD injection site, regions reciprocally connected with the SLD contained abundant αSyn aggregates at 12 mpi, which suggests delayed aggregation

in output regions following the transport of seeds along SLD connections. Our histological observations in the SLD resembles the pathological trajectory of neurons in the substantia nigra pars compacta in previous PFF inoculation studies,[23),54)] suggesting that SLD neurons may be comparable in their pathologic vulnerability as other PD-relevant nuclei. With respect to the relationship between pathology and behavioral symptoms, the onset of RBD-like behaviors preceded significant SLD neuronal loss, which suggests that PFF-induced pathology may cause SLD dysfunction that leads to RBD symptoms, prior to cell death. Consistent with this notion, PFF-induced synucleinopathy compromises the activity and synaptic function of neurons before affecting their viability,[55),56)] and merely preventing glutamate neurotransmission from SLD cells triggers an RBD-like phenotype in rodents.[40),57)] Collectively, these findings demonstrate that PFF injection into the SLD induced progressive synucleinopathy accompanied by neuronal loss, both of which are key neuropathological hallmarks of PD.

Neuropathological data also indicate that certain brain nuclei are selectively vulnerable to αSyn pathology in PD.[58)] We reasoned that RBD mechanisms could consist of the overlap between pathologically vulnerable and functionally relevant neuronal populations at the level of the SLD, prompting us to delineate the cellular substrates for RBD in this region. First, we demonstrate that targeted αSyn overexpression in SLD neurons caused RBD-like behaviors in mice. Previous basic science research has been focused on glutamatergic function in the SLD in REM sleep motor control. However, our findings suggest that αSyn aggregates in cholinergic neurons in the SLD and dysfunctional cholinergic neurotransmission would be the main pathomechanism of RBD in synucleinopathy. Injection of the cholinergic agonist carbachol into the dorsomedial pons produced an REM sleep-like state with muscle atonia and cortical activation.[59)] Patients with idiopathic RBD showed degeneration of cholinergic basal forebrain and reduced neocortical cholinergic denervation.[60),61)] Acetylcholinesterase inhibitor, such as donepezil and rivastigmine, showed an effect in controlling RBD.[62),63)] The association between αSyn pathology in human SLD or mesopontine cholinergic neuronal group and RBD should be investigated to elucidate the primary role of cholinergic dysfunction in the development of RBD in synucleinopathy including PD. Intriguingly, we observed that PFF injection induced αSyn accumulation in oligodendrocytes surrounding SLD neurons. Within the SLD, oligodendroglial pathology developed slower than in neurons, with abundant αSyn aggregates observed in SLD oligodendrocytes from 6 mpi.

Clinically, RBD is more prevalent in multiple system atrophy whose pathological hallmark is oligodendroglial cytoplasmic αSyn inclusions, than in PD.[64] However, the exact neural correlate and pathophysiology of RBD in multiple system atrophy has not yet been elucidated. Moreover, the prevalence of RBD in patients with PD is high and increases with disease severity.[65] Our data suggest that delayed oligodendroglial pathology in the SLD may contribute to the persistence of RBD phenotype in synucleinopathy after neuronal dysfunction in the SLD. Also, investigating the role of oligodendroglial αSyn pathology in RBD may give us a clue to understanding the common mechanism of RBD in synucleinopathies.

Following the initial seeding of αSyn pathology in SLD neurons, we observed its propagation to multiple distant brain regions over time. Pathological spread occurred broadly over the SLD connectome, resulting in αSyn aggregation in brain regions connected with the SLD.[66] Our findings can be taken with previous investigations, suggesting that neural connectivity is a major determinant of pathological progression.[25),55),67] Seeking to determine the consequences of αSyn propagation on behavior, we found that transmission of αSyn pathology to the substantia nigra pars compacta occurred at 6 mpi and gait deficits were observed at 12 mpi. The motor deficits were not attributable to weakened muscular strength as shown by normal grip strength measurements. Unexpectedly, PFF-injected mice performed similarly to controls on rotarod testing. However, the rotarod, which forces animals to run at high speeds, may be less sensitive for detecting subtle changes in ambulation.[68] It is also possible that more severe deficits would eventually emerge with extended post-injection intervals, given that RBD patients already experience subclinical motor dysfunction at prodromal stages,[69),70] that motor symptom severity increases with time, and that severe motor impairment does not typically develop until up to 60% of neurons in the substantia nigra pars compacta have been lost. Nonetheless, because disrupted gait is a core symptom of PD,[47] we have demonstrated that propagative α-synucleinopathy drives the conversion of an RBD-like into a Parkinsonian motor phenotype, recapitulating progression from prodromal to manifest stages of PD.

RBD is the prototypical sleep disturbance in prodromal PD, but patients commonly experience additional sleep-wake disturbances at advanced stages, including insomnia, sleep fragmentation, and impaired cortical activation.[45),71] In fact, these changes can present alongside RBD at

prodromal stages,[72),73)] and, like the severity of RBD symptoms, predict future motor and cognitive decline.[74),75)] This suggests that sleep disturbances are not only integral to the core symptomatology of PD but can themselves modulate disease progression. Despite this, previous animal models of RBD report no changes in sleep-wake architecture or EEG activity,[24),40),41)] and evidence for similar changes in models of PD is sparse.[76),77)] In our study, we demonstrate that PFF injection caused early RBD-like behaviors that were followed by reductions in NREM and REM sleep quantities and impaired cortical activation. Interestingly, midbrain lesions encompassing the substantia nigra in cats elicit both insomnia and waking motor deficits,[78)] suggesting that pathological spread to the substantia nigra alone could explain the simultaneous onset of gait deficits and sleep loss in our model. Considering the widespread distribution of PFF-induced pathology, it is more likely that such progressive dysregulation of sleep-wake behaviors, from initial RBD then to broader changes, reflects increasing pathologic involvement of many more sleep-wake circuits. Nevertheless, our model has recapitulated the progression of sleep disturbances throughout the course of PD, from an initial dissociation of REM sleep phenomena (RBD) which then proceeds to a more comprehensive breakdown of sleep-wake states.

This study has severe limitations. First, we could not elucidate which subneuronal populations were vulnerable to αSyn pathology in human SLD in parallel to mouse experiment. RNA-based in-situ hybridization using the target probe for Slc17a6 (VGLUT2) and Slc32a1 (VGAT) mRNA transcripts did not work well in human samples that have been fixed in formalin and stored for a long time. Second, the level total αSyn or SNCA mRNA was not measured in human SLD. Some previous studies have shown that these levels were elevated,[79),80),81)] which may be associated with the vulnerability to pathologic αSyn aggregates.[58)] Evaluation of total αSyn protein or SNCA expression level in the SLD may elucidate its specific role for RBD in synucleinopathies. Third, long-term follow-up for more than 12 months will be required to observe that this animal model would lead to the degeneration of nigral neurons to develop obvious motor deficits and to the occurrence of substantial cortical pathology to induce cognitive dysfunction. Fourth, we only measured glial pathology in the SLD. Since neuroinflammation is closely related to the propagation of αSyn pathology,[82)] the contribution of neuroinflammation beyond the SLD in the development of RBD needs to be investigated together.

In summary, our research provides novel insights into PD by illustrating how αSyn pathology within SLD neurons initiates RBD and contributes to its subsequent progression towards PD. This aligns with the hypothesis that PD progresses through a caudo-rostral transmission of pathology.[6] However, although the SLD is an early focus of PD pathology, the propagation patterns triggered by SLD inoculations may not fully represent the initial disease processes preceding RBD or the origins of αSyn pathology. Notably, RBD is suggested to arise from peripheral synucleinopathy.[83] This body-first hypothesis is substantiated by emerging imaging,[84),85] as well as biofluid or biopsy studies showing peripheral synucleinopathy in living RBD patients. Several studies have used PFFs to initiate αSyn propagation from peripheral sites in rodent models, but conclusive evidence linking peripheral αsyn seeding with RBD remains lacking. Moreover, it is unclear why RBD precedes distinct synucleinopathies and how a single pathological protein can give rise to diverse clinical outcomes. Disease-specific αSyn conformational strains are thought to explain the variability among synucleinopathies, but this concept has yet to be explored in the context of RBD. To conclude, this work has extended our understanding of RBD mechanisms, and we anticipate that our model will be useful for studying prodromal disease mechanisms in future investigations.

References

1) Dauer, W. & Przedborski, S. Parkinson's Disease: Mechanisms and Models. Neuron 2023:39;889-909.
2) Dickson, D. W. *et al*. Neuropathological assessment of Parkinson's disease: refining the diagnostic criteria. Lancet Neurol 2009;8:1150-1157.
3) Spillantini, M. G. *et al*. α-Synuclein in Lewy bodies. Nature 1997;388:839-840.
4) Singleton, A. B. *et al*. alpha-Synuclein locus triplication causes Parkinson's disease. Science 2003;302:841.
5) Lang, A. E. & Lozano, A. M. Parkinson's disease. N Eng J Med 1998;339:1044-1053.
6) Braak, H. *et al*. Staging of brain pathology related to sporadic Parkinson's disease. Neurobiol Aging 2003;24:197-211.
7) Beach, T. G. *et al*. Multi-organ distribution of phosphorylated alpha-synuclein histopathology in subjects with Lewy body disorders. Acta Neuropathol 2010;119:689-702.
8) Adler, C. H. & Beach, T. G. Neuropathological basis of nonmotor manifestations of Parkinson's disease. Mov Disord 2016:31;1114-1119.
9) Li, J. Y. *et al*. Lewy bodies in grafted neurons in subjects with Parkinson's disease suggest host-to-graft disease propagation. Nat Med 2008;14:510-503.
10) Boeve, B. F. *et al*. Pathophysiology of REM sleep behavior disorder and relevance to neurodegenerative disease. Brain 2007;130:2770-2788.
11) McKenna, D. & Peever, J. Degeneration of rapid eye movement sleep circuitry underlies rapid eye movement sleep behavior disorder. Mov Disord 2017;32:636-644.
12) Iranzo, A., Santamaria, J. & Tolosa, E. Idiopathic rapid eye movement sleep behaviour disorder: diagnosis, management, and the need for neuroprotective interventions. Lancet Neurol 2016;15:405-419.
13) Iranzo, A. *et al*. Neurodegenerative disease status and post-mortem pathology in idiopathic rapid-eye-movement sleep behaviour disorder: an observational cohort study. Lancet Neurol 2013;12:443-435.
14) Boeve, B. F. *et al*. Insights into REM sleep behavior disorder pathophysiology in brainstem-predominant Lewy bod disease. Sleep Med 2007;8:60-64.
15) Unger, M. M. *et al*. Diffusion tensor imaging in idiopathic REM sleep behavior disorder

reveals microstructural changes in the brainstem, substantia nigra, olfactory region, and other brain regions. Sleep 2010;33:767.
16) Scherfler, C. *et al*. White and gray matter abnormalities in idiopathic rapid eye movement sleep behavior disorder: a diffusion-tensor imaging and voxel-based morphometry study. Ann Neurol 2011;69:400-407.
17) Ehrminger, M. *et al*. The coeruleus/subcoeruleus complex in idiopathic rapid eye movement sleep behaviour disorder. Brain 2016;139:1180-1188.
18) Peever, J., Luppi, P.-H. & Montplaisir, J. Breakdown in REM sleep circuitry underlies REM sleep behavior disorder. Trends Neurosci 2014;37:279-288.
19) Meredith, G. E. & Rademacher, D. J. MPTP mouse models of Parkinson's disease: and update. J Parkinsons Dis 2011;1:19-33.
20) Thiele, S. L., Warre, R. & Nash, J. E. Development of a unilaterally-lesioned 6-OHDA mouse model of Parkinson's disease. J Vis Exp 2012;14:3234.
21) Henrich, M. T. *et al*. A53T-α-synuclein overexpression in murine locus coeruleus induces Parkinson's disease-like pathology in neurons and glia. Acta Neuropathol Commun 2018;6:39.
22) Decressac, M., Mattsson, B., Lundblad, M., Weikop, P. & Björklund, A. Progressive neurodegenerative and behavioural changes induced by AAV-mediated overexpression of α-synuclein in nigral dopamine neurons. Neurobiol Dis 2012;45:939-953.
23) Luk, K. C. *et al*. Pathological α-synuclein transmission initiates Parkinson-like neurodegeneration in nontransgenic mice. Science 2012;338:949-953.
24) Shen, Y. *et al*. Propagated α-synucleinopathy recapitulates REM sleep behaviour disorder followed by parkinsonian phenotypes in mice. Brain 2020;143:3374-3392.
25) Henrich, M. T. *et al*. Determinants of seeding and spreading of α-synuclein pathology in the brain. Sci Adv 2020;6:eabc2487.
26) Nomura, T., Inoue, Y., Kagimura, T., Uemura, Y. & Nakashima, K. Utility of the REM sleep behavior disorder screening questionnaire (RBDSQ) in Parkinson's disease patients. Sleep Med 2011;12:711-713.
27) Volpicelli-Daley, L. A., Luk, K. C. & Lee, V. M. Y. Addition of exogenous α-synuclein preformed fibrils to primary neuronal cultures to seed recruitment of endogenous α-synuclein to Lewy body and Lewy neurite-like aggregates. Nat Protoc 2014;9:2135-2146.
28) Torontali, Z. A., Fraigne, J. J., Sanghera, P., Horner, R. & Peever, J. The sublaterodorsal

tegmental nucleus functions to couple brain state and motor activity during REM sleep and wakefulness. Curr Biol 2019;29:3803-3813.e5.
29) Fraigne, J. J. *et al*. A novel machine learning system for identifying sleep-wake states
30) McCarter, S. J. *et al*. Diagnostic thresholds for quantitative REM sleep phasic burst duration, phasic and tonic muscle activity, and REM atonia index in REM sleep behavior disorder with and without comorbid obstructive sleep apnea. Sleep 2014;37:1649-1662.
31) Silvani, A. *et al*. Muscle activity during sleep in human subjects, rats, and mice: towards translational model of REM sleep without atonia. Sleep 2017;40.
32) Blumberg, M. S. & Plumeau, A. M. A new view of “dream enactment” in REM sleep behavior disorder. Sleep Med Rev 2016;30:34-42.
33) Arnulf, I. REM sleep behavior disorder: motor manifestations and pathophysiology. Mov Disord 2012;27:677-689.
34) Brooks, P. L. & Peever, J. A temporally controlled inhibitory drive coordinates twitch movements during REM sleep. Curr Biol 2016;26:1177-1182.
35) Yates, S. C. *et al*. QUINT: Workflow for quantification and spatial analysis of features in histological images from rodent brain. Front Neuroinform 2019;13:75.
36) Carey, H. *et al*. DeepSlice: rapid fully automatic registration of mouse brain imaging to a volumetric atlas. Nat Commun 2023;14:5884.
37) Nutil: A pre- and post-processing toolbox for histological rodent brain section images. Front Neuroinform 2020;14:37.
38) Motulsky, H. J. & Brown, R. E. Detecting outliers when fitting data with nonlinear regression – A new method based on robust nonlinear regression and the false discovery rate. BMC Bioinformatics 2006;7:1-20.
39) Sastre, P. J. P. & Jouvet, M. Le comportement onirique du chat. Physiol Behav 1979;22:979-989.
40) Garcia, S. V. *et al*. Genetic inactivation of glutamate neurons in the rat sublaterodorsal tegmental nucleus recapitulates REM sleep behaviour disorder. Brain 2017;140:414-428.
41) Taguchi, T. *et al*. A-Synuclein BAC transgenic mice exhibit RBD-like behaviour and hyposmia: a prodromal Parkinson’s disease model. Brain 2020;143:249-265.
42) Rey, N. L. *et al*. Widespread transneuronal propagation of α-synucleinopathy triggered in olfactory bulb mimics prodromal Parkinson’s disease. J Exp Med 2016;213:1759-1778.

43) Cygan, F., Oudiette, D., Leclair-Visonneau, L., Leu-Semenescu, S. & Arnulf, I. Night-to-night variability of muscle tone, movements, and vocalizations in patients with REM sleep behavior disorder. J Clin Sleep Med 2010;6:551-555.
44) Breen, D. P. *et al*. Sleep and circadian rhythm regulation in early Parkinson's disease. JAMA Neurol 2014;71:589-595.
45) French, I. T. & Muthusamy, K. A. A review of sleep and its disorders in patients with Parkinson's disease in relation to various brain structures. Front Aging Neurosci 2016;8:175540.
46) Boeve, B. F. Idiopathic REM sleep behaviour disorder in the development of Parkinson's disease. Lancet Neurol 2013;12:469-482.
47) Zanardi, A. P. J. *et al*. Gait parameters of Parkinson's disease compared with healthy controls: a systematic review and meta-analysis. 2021;11:752.
48) Simuni, T. *et al*. A biological definition of neuronal α-synuclein disease: towards an integrated staging system for research. Lancet Neurol 2024;23:178-190.
49) Höglinger, G. U. *et al*. A biological classification of Parkinson's disease: the SynNeurGe research diagnostic criteria. Lancet Neurol 2024;23:191-204.
50) Lu, J., Sherman, D., Devor, M. & Saper, C. B. A putative flip-flop switch for control of REM sleep. Nature 2006;441:589-594.
51) Anaclet, C., Pedersen, N. P., Fuller, P. M. & Lu, J. Brainstem circuitry regulating phasic activation of trigeminal motoneurons during REM sleep. PLoS One 2010;5:e8788.
52) American Academy of Sleep Medicine. International Classification of Sleep Disorders: Diagnostic and Coding Manual. 3rd Ed. 2014.
53) Nepozitek, J. *et al*. Magnetic susceptibility changes in the brainstem reflect REM sleep without atonia severity in isolated REM sleep behavior disorder. NPJ Parkinsons Dis 2023;9:112.
54) Rahayel, S. *et al*. Differentially targeted seeding reveals unique pathological alpha-synuclein propagation patterns. Brain 2022;145:1743-1756.
55) Volpicelli-Daley, L. A. *et al*. Exogenous α-synuclein fibrils induce Lewy body pathology leading to synaptic dysfunction and neuron death. Neuron 2011;72:57-71.
56) Wu, Q. *et al*. α-synuclein (αSyn) preformed fibrils induce endogenous αSyn aggregation, compromise synaptic activity and enhance synapse loss in cultured excitatory hippocampal neurons. J Neurosci 2019;39:5080-5094.
57) Krenzer, M. *et al*. Brainstem and spinal cord circuitry regulating REM sleep and muscle

atonia. PLoS One 2011;6:e24998.
58) Surmeier, D. J., Obeso, J. A. & Halliday, G. M. Selective neuronal vulnerability in Parkinson disease. Nat Rev Neurosci 2017;18:101-113.
59) Weng, F. J. *et al*. Carbachol excites sublaterodorsal nucleus neurons projecting to the spinal cord. J Physiol 2014;592:1601-1617.
60) Tan, C. *et al*. Cholinergic nucleus 4 degeneration and cognitive impairment in isolated rapid eye movement sleep behavior disorder. Mov Disord 2023;38:474-479.
61) Stokholm, M. G. *et al*. Cholinergic denervation in patients with idiopathic rapid eye movement sleep behaviour disorder. Eur J Neurol 2020;27:644-652.
62) Ringman, J. M. & Simmons, J. H. Treatment of REM sleep behavior disorder with donepezil: a report of three cases.
63) Giacopo, R. D. *et al*. Rivastigmine as alternative treatment for refractory REM behavior disorder in Parkinson's disease. Mov Disord 2012;27:559-561.
64) Baumann-Vogel, H. *et al*. REM sleep behavior in Parkinson disease: Frequent, particularly with higher age. PLoS One 2020;15:e0243454.
65) Sixel-Döring, F. *et al*. The increasing prevalence of REM sleep behavior disorder with Parkinson's disease progression: a polysomnography-supported study. Mov Disord Clin Pract 2023;10:1769-1776.
66) Boissard, R., Fort, P., Gervasoni, D., Barbagli, B. & Luppi. P. H. Localization of the GABAergic and non-GABAergic neurons projecting to the sublaterodorsal nucleus and potentially gating paradoxical sleep onset. Eur J Neurosci 2003;18:1627-1639.
67) Henderson, M. X. *et al.* Spread of α-synuclein pathology through the brain connectome is modulated by selective vulnerability and predicted by network analysis. Nat Neurosci 2019;22:1248-1257.
68) Tatenhorst, L. *et al*. Fasudil attenuates aggregation of α-synuclein in models of Parkinson's disease. Acta Neuropathol Commun 2016;4:39.
69) Fereshtehnejad, S. M. *et al*. Evolution of prodromal Parkinson's disease and dementia with Lewy bodies: a prospective study. Brain 2019;142:2051-2067.
70) Postuma, R. B. *et al*. Risk and predictors of dementia and parkinsonism in idiopathic REM sleep behaviour disorder: a multicentre study. Brain 2019;142:744-759.
71) Breen, D. P. *et al*. Sleep and circadian rhythm regulation in early Parkinson disease. JAMA

Neurol 2014;71:589-595.
72) Lai, Y. Y. & Siegel, J. M. Physiological and anatomical link between Parkinson-like disease and REM sleep behavior disorder. Mol Neurobiol 2003;27:137-151.
73) Fantini, M. L. *et al*. Slowing of electroencephalogram in rapid eye movement sleep behavior disorder. Ann Neurol 2003;53:774-780.
74) Lysen, T. S., Darweesh, S. K. L., Kamran Ikram, M., Luik, A. I. & Arfan Ikram, M. Sleep and risk of parkinsonism and Parkinson's disease: a population-based study. Brain 2019;142:2013-2022.
75) Liang, J. *et al*. Short sleep duration is associated with worse quality of life in Parkinson's disease: A multicenter cross-sectional study. Sleep Med 2024;114:182-188.
76) McDowell, K. A., Shin, D., Roos, K. P. & Chesselet, M. F. Sleep dysfunction and EEG alterations in mice overexpressing alpha-synuclein. J Parkinsons Dis 2014;4:531-539.
77) Summa, K. C. *et al*. Disrupted sleep-wake regulation in the MCI-Park mouse model of Parkinson's disease. NPJ Parkinsons Dis 2024;10:1-9.
78) Lai, Y. Y. *et al*. Neurotoxic N-methyl-D-aspartate lesion of the ventral midbrain and mesopontine junction alters sleep-wake organization. Neuroscience 1999;90:469-483.
79) Öhrfelt, A. *et al*. Identification of novel α-synuclein isoforms in human brain tissue by using an online NanoLC-ES1-FTICR-MS method. Neurochem Res 2011;36:2029.2042.
80) Moors, T. E. *et al*. Multi-platform quantitation of alpha-synuclein human brain proteoforms suggests disease-specific biochemical profiles of synucleinopathies. Acta Neuropathol Commun 2022;10:82.
81) Chiba-Falek, O., Lopez, G. J. & Nussbaum, R. L. Levels of alpha-synuclein mRNA in sporadic Parkinson disease patients. Mov Disord 2006;21:1703-1708.
82) Kim T. K. et al. Inflammation promotes synucleinopathy propagation. Exp Mol Med 2022;54:2148-2161.
83) Borghammer, P. The α-Synuclein Origin and Connectome Model (SOC Model) of Parkinson's Disease: Explaining Motor Asymmetry, Non-Motor Phenotypes, and Cognitive Decline. J Parkinsons Dis 2021;11:455-474.
84) Horsager, J. et al. Brain-first versus body-first Parkinson's disease: a multimodal imaging case-control study. Brain 2020;143:3077-3088.
85) Knudsen, K. et al. In-vivo staging of pathology in REM sleep behaviour disorder: a

multimodality imaging case-control study. Lancet Neurol 2018;17:618-628.

Abstract in Korean

파킨슨병 전구증상으로써의 알파시누클린 피브릴 기반 렘수면 행동장애 생쥐 모델 개발

배경 및 목적: 렘수면 행동장애는 알파시누클린병증 발생을 강력하게 예측하는 증상으로 잘 알려져 있다. Sublaterodorsal tegmental nucleus (SLD)는 렘수면 동안 근육 무긴장을 유지하는 데 중요한 역할을 한다. 렘수면 행동장애의 근본적인 기전은 아직 알려지지 않았으나, 이는 알파시누클린에 의한 SLD 신경세포의 퇴행에 기인하는 것으로 생각된다. 따라서 알파시누클린병증을 통합하고 렘수면 행동장애를 재현하는 동물 모델을 개발하면 알파시누클린병증의 전구 단계를 연구할 수 있겠다. 야생형 마우스에서 알파시누클린 피브릴을 SLD에 주입한 후 렘수면 행동장애 및 그에 따른 파킨슨병과 유사한 표현형이 나타나는지를 이 연구를 통하여서 조사하였다.

방법: 인간 부검 샘플을 사용하여 루이소체질환 환자의 렘수면 행동장애 동반에 따라 SLD의 알파시누클린 병리의 정도를 조사하였다. 아데노 관련 바이러스를 사용하여 SLD 신경세포에서 알파시누클린의 과발현을 유도하여 SLD에서 알파시누클린 병리과 렘수면 행동장애의 발생 간의 인과관계를 확립하였다. 그런 다음 야생형 마우스 알파시누클린 피브릴을 B6C3F1/J 마우스의 SLD에 주입하고, 정해진 시점에서 마우스의 조직병리, 전기생리학적 특성 및 행동 분석을 시행하였다. 인산화된 알파시누클린 및 신경전달물질 표지자에 대한 항체를 사용하여 알파시누클린 병리가 어떤 신경세포에 잘 축적되는지를 밝혔고, 신경세포 및 교세포 표지자를 사용하여서 SLD에서 신경의 퇴행과 반응성 신경교증을 조사하였다.

결과: 인산화된 알파시누클린에 대한 면역조직화학 염색을 통하여서 렘수면 행동장애를 동반한 파킨슨병 환자의 SLD에 알파시누클린 응집체가 많을 것을 관찰하였고, 반면에

렘수면 행동장애가 없는 파킨슨병 환자나 건강한 대조군에서는 응집체가 희소하거나 없었다. SLD 신경세포에서 아데노 관련 바이러스를 이용한 알파시누클린의 과발현은 마우스에서 렘수면 행동장애와 유사한 행동을 유도하였다. 마우스 SLD에 알파시누클린 피브릴을 주입했을 내인성 알파시누클린 병리가 발생하였고 주입 부위로부터 위로는 대뇌 피질로, 아래로는 척수로 병리가 전파됨을 관찰하였다. 특별히, 흑색질 병리는 주사 6개월째 발견되었다. 병리적 응집체는 초기에는 콜린성 신경세포에서 발견이 되었고 시간이 지나면서 SLD 신경세포 주변의 희소돌기아교세포(oligodendrocyte)에서도 발견이 되었다. SLD내 파종된 알파시누클린 병리는 주사 3개월째부터 마우스에서 렘수면 행동장애와 유사한 행동과 연관을 보였고, 6개월째부터 피질 둔화 및 교란된 수면-각성 구조를 보였다. 전파된 알파시누클린 병리는 12개월째 보행 결손을 유발하였고 특이 수컷에서 뚜렷한 차이를 보였다.

결론: 우리는 SLD가 알파시누클린병의 조기 확산을 위한 포탈(portal) 역할을 할 수 있고, 이런 방식으로 유도한 알파시누클린 병리는 마우스에서 렘수면 행동장애와 유사한 표현형을 나타낸다는 것을 보여줬다. 우리는 이 마우스 모델이 파킨슨병을 포함한 알파시누클린병증에서 전구 질환의 기전을 이해하고 질병을 조절할 수 있은 치료법을 연구하는 데에 유용한 도구가 될 것으로 기대한다.

핵심되는 말 : 렘수면 행동장애; 파킨슨병; sublaterodorsal tegmental nucleus; 알파시누클린; 마우스 모델.